Mem. S.A.It. Vol. 94, 105

Memorie della

Sources of r-Process Abundances

F.-K. Thielemann[1,2], K. Farouqi[3], S. Rosswog[4,5], and K.-L. Kratz[6]

[1] University of Basel, Department of Physics, Klingelbergstrasse 82, CH-4056 Basel, Switzerland, e-mail: f-k.thielemann@unibas.ch
[2] GSI Helmholtz Center for Heavy Ion Research, Planckstrasse 1, D-64291 Darmstadt, Germany
[3] ZAH, Landessternwarte, University of Heidelberg, Königstuhl 12, D-69117 Heidelberg, Germany
[4] Hamburger Sternwarte, Gojenbergsweg 112, Room 013, Grosses Beamtenwohnhaus, 21029 Hamburg, Germany
[5] Department of Astronomy & Oskar Klein Centre, Stockholm University, SE-106 91, Stockholm, Sweden
[6] University of Mainz, Department of Chemistry, Pharmacy & Geosciences, D-55126 Mainz, Germany

Received: 21-11-2022; Accepted: 23-11-2022

Abstract. A major question related to the evolution of heavy element abundances during galactic evolution is whether the r-process composition as found in the solar system is coming from a unique type of astrophysical event or whether it presents a superposition of different contributions. Up to now a neutron star merger GW170817 is the the only observationally identified r-process site. However there exist also other suggestions for r-process sources, like (rare classes of?) supernovae, hypernovae/collapsars, as well as neutron star - black hole mergers. We present predictions resulting from theoretical modeling of such events and try to search for their imprint in low metallicity stars, when the r-process still dominates over the s-process for heavy element abundances. Early galactic evolution and variations in observed nucleosynthesis signatures, e.g. limited-r stars, r-process enriched r-I and r-II stars, as well as actinide boost stars, might indicate the need for such other sites.

Key words. nuclear reactions, nucleosynthesis, abundances – supernovae: general – stars: abundances – Galaxy: evolution

1. Introduction

A number of contributions to this conference have summarized the status of element abundance observations in low-metallicity stars. Here we want to focus on their r-process contributions and discuss first the nucleosynthesis working of the r-process, the possible astrophysical sites, and the related abundance predictions. Then we address also their occurrence frequency and their impact on the time evolution throughout galactic history, with the aim to provide an understanding how these individual sites enter the evolution of the Galaxy. The goal is to find ways: (a) how to identify the astrophysical site(s) responsible for the individual features and variations in observed abundance patterns during galactic evolution and (b) how all sites act in a combined way,

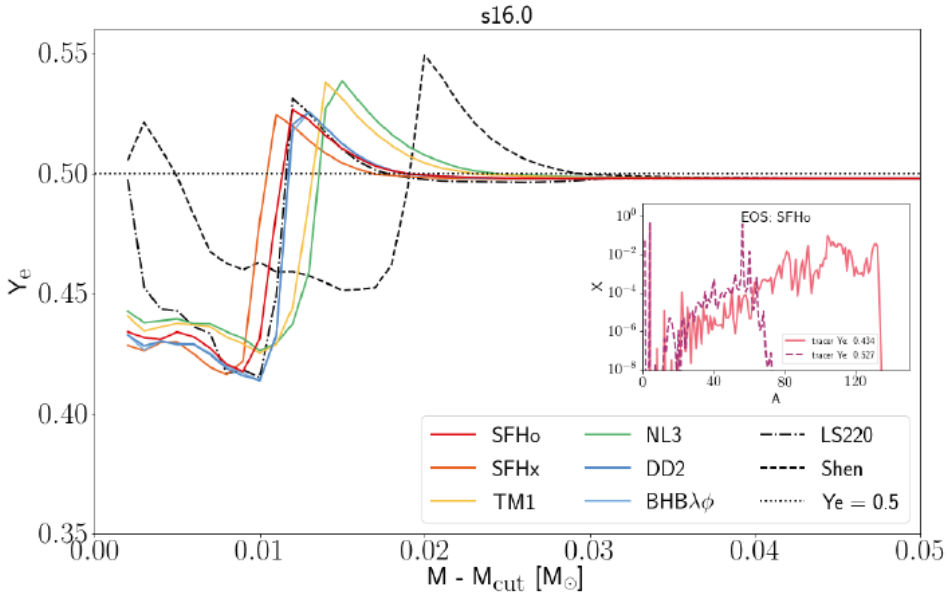

Fig. 1. Innermost ejecta composition determined by (a) moderately low Y_e-matter from collapse and (b) moderately proton-rich conditions due to neutrino interactions during the explosion, leading to a very weak r-process and a νp-process (collapse calculations performed with different equations of state). Image reproduced with permission from Ghosh et al. (2022), copyright by the authors.

resulting in the overall solar r-process abundances. For these reasons we present first the individual suggested nucleosynthesis sites (for more details see our reviews Cowan et al. 2021; Arcones & Thielemann 2022) and will then focus on the question how one can identify their joint imprint in galactic evolution as a function of metallicity [Fe/H] (for more details see Farouqi et al. 2022).

2. Suggested r-process sites

2.1. Core-collapse supernovae

Core-collapse marks the end of the life of stars with at least 8 $M_\odot$, leading to the birth of neutron stars and/or stellar-mass black holes. In observations one notices a variation in explosion energies, dividing them into two categories: low and high energy explosion (i.e. core-collapse supernovae and hypernovae). Core-collapse supernovae are triggered by neutrinos that deposit the energy released from the hot proto-neutron star (emerging from core-collapse) in the stalled shock with the help of convection and instabilities (Burrows 2013; Kotake et al. 2012; Janka et al. 2016; Müller 2016; Radice et al. 2018; Müller 2020; Burrows & Vartanyan 2021; Vartanyan et al. 2022; Varma et al. 2022). Here we summarize only briefly the rich nucleosynthesis occurring in the innermost ejected zones which are prone to eject heavy elements beyond the Fe-group.

A complete prediction of the nucleosynthesis in neutrino-driven ejecta needs a large number of three-dimensional simulations, following the explosion for a few seconds and for different progenitors. This requires exhaustive computational efforts and also still involves uncertain details of the explosion. On the other hand, traditional spherically symmetric methods (like artificial piston or thermal or kinetic bomb approaches) are not suitable for the nucleosynthesis of the innermost zones that de-

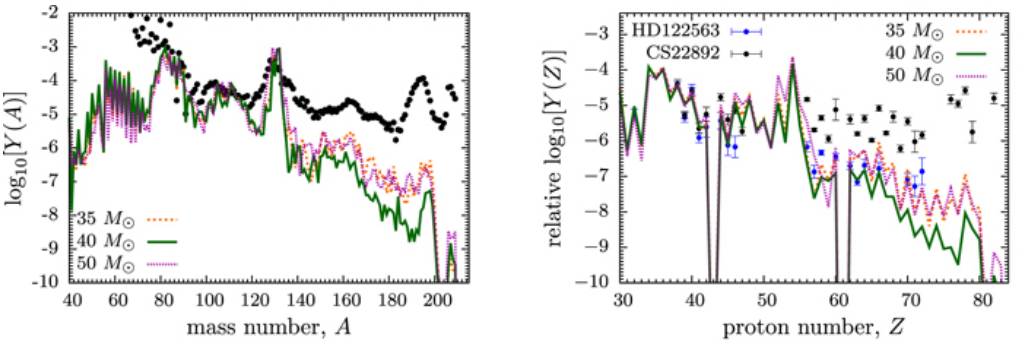

(a) Isotopic abundances in comparison to solar (black dots)

(b) Elemental abundances in comparison to metal-poor stars

Fig. 2. Ejecta composition of quark-deconfinement supernovae as a function stellar progenitor mass, In all cases a weak r-process is attained, mostly with abundances up to the 130 peak. Also heavier nuclei are produced, however, on an almost negligble level. The left panel compares isotopic abundance with solar r-process abundances, the right panel with element abundances in comparison to an r-enriched r-II and a limited-r star (representing a weak r-process site). Image reproduced with permission from Fischer et al. (2020), copyright by AAS.

pends on the Y_e and thus on detailed neutrino transport. Approximate methods to obtain neutrino-driven explosions have been undertaken, e.g. within the PUSH approach (Perego et al. 2015; Curtis et al. 2019; Ebinger et al. 2020; Ghosh et al. 2022), based on a modified neutrino heating deduced from full multi-D models.

In Fig.1 we show the results of Ghosh et al. (2022), which indicate two important features: (a) there exist ejecta which inherit some slightly neutron-rich features $Y_e < 0.5$ from the core-collapse phase which led via electron capture to a strong neutronization of matter and (b) the neutrino interaction with matter, causing the final explosion with enhanced Y_e, because of the two neutrino capture reactions $\nu_e + n \rightarrow p + e^-$ and $\bar{\nu}_e + p \rightarrow n + e^+$. For similar neutrino and antineutrino energies the first reaction wins due to the neutron-proton mass difference. The two nucleosynthesis features related to both conditions are a (very?) weak r-process, producing possibly nuclei up to the A=130 peak, and a νp-process (working via proton captures and (n,p)-reactions, Fröhlich et al. 2006) up to $A \approx 70$.

2.2. Quark-deconfinement supernoave

Quark-deconfinment supernovae have been proposed for a while (Fischer et al. 2011; Fischer et al. 2020). Dependent on the nuclear equation of state for massive core-collapse events, the collapse of the proto-neutron star to a black hole can be avoided (in a specific stellar mass range) due to a quark-hadron phase transition with the right characteristics. This leads to a stable central quark core and a successful supernovae explosion, based on the bounce shock (and neutrino energy deposition) which permits to eject mildly neutron-rich matter. Such events (taking place for certain equation of state choices - but consistent with present experimental constraints - and in a specific stellar mass range) would experience a weak r-process, also producing sufficient nuclei up to the A=130 peak, but populating even the actinides (see Fig.2), however, with negligible abundances (Fischer et al. 2020).

2.3. Magneto-rotational supernovae

In addition to neutrino-driven explosions, observations of very energetic supernovae (Nomoto et al. 2010), long gamma-ray bursts (GRBs, Woosley & Bloom 2006), and neutron stars with extremely high magnetic fields

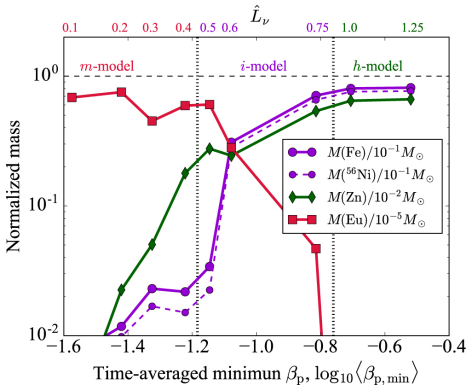

Fig. 3. Ejected masses of Fe, ^{56}Ni (before decay), Zn, and Eu, normalized by 0.1, 10^{-2}, and 10^{-5} $M_\odot$, respectively, as a function of the initial magnetic field strength and related neutrino luminosity. Image reproduced with permission from Nishimura et al. (2017), copyright by AAS.

(magnetars, Kramer 2009; Greiner et al. 2015) indicate the key role of magnetic fields in some explosions. Here we focus on magneto-rotational supernovae (MR SNe), leading to a magnetized neutron star remnant, starting with rapid rotation of the iron core before collapse and experiencing an amplification of the magnetic field by rotational winding and/or the magneto-rotational instability (MRI) (Obergaulinger et al. 2009). After bounce, the strong magnetic pressure launches jets along the rotational axis (Burrows et al. 2007; Takiwaki et al. 2009; Winteler et al. 2012; Mösta et al. 2014; Obergaulinger et al. 2014; Nishimura et al. 2015, 2017; Reichert et al. 2021, 2022). If simulations are performed in 3D, kink instabilities can set in, delay the explosion, and cause the formation of less collimated bipolar jets (Mösta et al. 2014, 2018; Kuroda et al. 2020).

Nishimura et al. (2015, 2017) have explored the impact on the nucleosynthesis of different magnetic field strengths and rotation rates. Fig.3 shows the results of Nishimura et al. (2017), which vary parametrically the initial magnetic field strength and rotation, leading to variations in neutrino heating from the proto-neutron star. This variation causes a transition from a behavior close to a regular core collapse supernova (with high Ni(Fe) and Zn ejecta) to highly neutron-rich ejecta with a large Eu production. To summarize the nucleosynthesis aspects of ejected matter from MR SNe, one should point out that initial hopes to have a full-fledged strong r-process (Winteler et al. 2012) are only partially confirmed in more realistic simulations. The strong r-process depends on a very high magnetic field strength of the rotating core before collapse. This permits to have a fast ejection of neutron-rich matter. If the magnetic fields are weaker and get enhanced only by magneto-rotational instabilities (MRI) during the onset of the explosion, this permits neutrinos streaming out from the proto-neutron star to enhance the Y_e of the ejecta and consequently reduces the strength of an r-process. The latter corresponds to the intermediate case (i) of Fig.3, while case (m) stands for very strong initial magnetic fields and case (h) is close to a regular core-collapse supernova.

2.4. Collapsars

Other potential r-process sites are collapsars, associated with the collapse of rotating massive stars, finally ending in a central black hole, jet ejection - accompanied by a long duration gamma-ray burst - and an accretion disc that forms surrounding the massive central black hole. Pioneering nucleosynthesis studies (Surman & McLaughlin 2004; McLaughlin & Surman 2005; Surman et al. 2006) have demonstrated that also here neutrinos can play a critical role, reducing the neutron-richness of the ejecta. The possibilities for an r-process are not conclusive, yet. However, based on the general-relativistic MHD simulations discussed below, Farouqi et al. (2022) explored this line of investigations.

An interesting question is related to whether some environments can actually lead to a strong r-process with a so-called actinide boost in the ejected abundances, while other objects produce just a normal solar-type r-process distribution. Recent studies (Holmbeck et al. 2019b), based on a hydrodynamic ejecta trajectory, conclude that actinides are substantially overproduced relative to lanthanides for

Y_e-values in the range 0.1–0.15, due to the influence of fission cycling. This is consistent with Wu et al. (2017) and a recent study of Eichler et al. (2019), i.e. "actinide boost" compositions require a dominant fraction of the ejecta to originate from a very narrow Y_e-range. What kind of environment can lead to such a robust behavior? A possibility was recently suggested by Farouqi et al. (2022). If a black hole forms this leads to an accretion disk with an electron fractions of $Y_e \approx 0.1$ (Beloborodov 2003). This occurs once the accretion rates exceed a critical value depending on the BH spin (Chen & Beloborodov 2007), which correspond to accretion rates which power long GRBs (Lee & Ramirez-Ruiz 2007). Y_e-values of ≈ 0.1 are found in full-fledged numerical (magneto-) hydrodynamic simulations (see e.g., Siegel & Metzger 2018; Fernández et al. 2019). The simulation of such neutrino-cooled accretion flows is a major challenge. Currently existing general relativistic magneto-hydrodynamic GRMHD explorations (Siegel & Metzger 2017; Siegel & Metzger 2018; Miller et al. 2020; Fernández et al. 2019) agree that a large fraction ($\sim 40\%$) of the initial torus mass becomes unbound. Fernández et al. (2019) find Y_e values around 0.12, those of Siegel & Metzger (2018) peak around ~ 0.14, while Miller et al. (2020) find a broad distribution between 0.2 and 0.4. Despite these remaining uncertainties Farouqi et al. (2022) suggested that black hole tori could be the source of "actinide boost" material. Fig.4 includes abundance predictions resulting from ejecta with Y_e-values in the range 0.1-0.15, as discussed above (Wu et al. 2017; Thielemann et al. 2020).

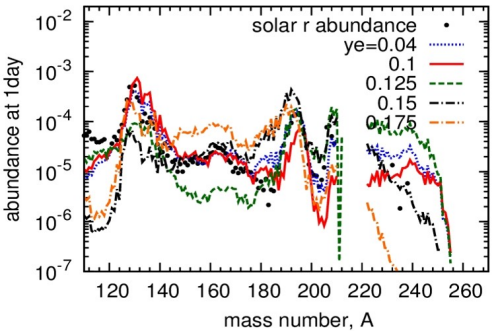

Fig. 4. Utilizing the DZ (Duflo-Zucker) mass model (Duflo & Zuker 1995) one sees large variations of actinide production as a function of Y_e in the ejecta. The highest actinide production takes place for a range of 0.125 to 0.15, decreasing strongly for higher as well as lower $Y_e's$ (Wu et al. 2017). Image reproduced with permission from Thielemann et al. (2020), copyright by the authors.

2.5. Compact binary mergers

The initial search for a unique type of event that reproduces exactly the solar r-process abundances included especially neutron star mergers (Lattimer & Schramm 1974, 1976; Eichler et al. 1989). Concrete predictions for resulting abundance features were reviewed by Thielemann et al. (2017) before the gravitational wave event GW170817 (Abbott et al. 2017), which was accompanied by an r-process powered kilonova (Metzger et al. 2010; Rosswog et al. 2018; Zhu et al. 2018; Metzger 2019). The transition from an initially blue to a red appearance could be explained by the following effects. Early on elements lighter than barium (Z = 56) with a low density of atomic levels dominate (Kasen et al. 2017), being accompanied by the detection of Sr (Watson et al. 2019). The later red appearance indicates the presence of lanthanides and actinides, both aspects have completed our understanding (see for further reviews and recent results e.g. Horowitz et al. 2019; Shibata & Hotokezaka 2019; Metzger 2019; Cowan et al. 2021; Perego et al. 2021; Shibata et al. 2021; Rosswog & Korobkin 2022; Fujibayashi et al. 2022; Perego et al. 2022; Curtis et al. 2022).

Based on these considerations, three components of neutron star merger ejecta contribute to the overall nucleosynthesis site: (i) dynamical ejecta, including compressed and shock heated material from the initial collision as well as possible – cold – tidal spiral arm-type ejecta, (ii) winds driven by neutrinos, emitted from the central hot (hypermassive but supported by rotation?) neutron star and the accretion disk, and (iii) finally mass outflow from the accretion disk (see e.g. Figs.5 and 6). A common feature of these scenarios is that mat-

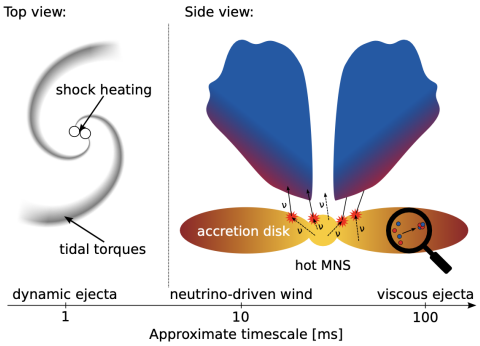

Fig. 5. Schematic representation of a neutron star merger and its ejecta, from Arcones & Thielemann (2022), copyright by the authors.

ter reaches NSE with Y_e given by weak reactions or by beta equilibrium in the cold tidal ejecta.

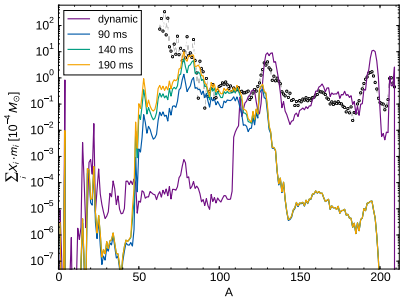

Fig. 6. Elemental abundance comparison between BNS merger models and metal poor star observations. The violet curve represents nucleosynthesis yields for tidally dominated dynamical ejecta (Korobkin et al. 2012), while the other curves represent yields from neutrino-driven wind ejecta for different massive NS lifetimes. Theoretical abundances are compared with solar r-process ejecta. Images reproduced with permission from Martin et al. (2015), copyright by AAS.

Combining the three types of ejecta, there is no doubt that neutron star mergers are indeed a major r-process source (Evans et al. 2017; Wu et al. 2019; Kasliwal et al. 2022; Perego et al. 2022; Curtis et al. 2022). Variation in nucleosynthesis conditions have been predicted by Wanajo et al. 2014; Just et al. 2015; Martin et al. 2015; Wu et al. 2016; Bauswein et al. 2017; Miller et al. 2019; Barnes et al. 2021; Lund et al. 2022). In summary, there is strong evidence that this neutron star merger event has produced at least a broad, and maybe the whole, r-process range. However, based on the observed lanthanide fraction $X_{\rm La}$, Ji et al. (2019) find that for the neutron star merger GW170817 this does probably not represent a typical solar r-process pattern.

3. Galactic chemical evolution

Stellar (surface) abundances are inherited from the interstellar medium in which the stars were born, i.e. one can look back in time. The early phases of galactic evolution are characterized by a large degree of abundance scatter and spatial inhomogeneities, which cannot be explained by traditional chemical evolution studies (Matteucci et al. 2014). To account for this, inhomogeneous "chemical evolution" models do not assume that ejecta mix completely and instantaneously with the whole galactic interstellar medium. Instead, they consider only the pollution of about 5×10^4 $M_\odot$ (via a Sedov-Taylor blast wave) of the interstellar medium (see e.g. Cescutti et al. 2015; Wehmeyer et al. 2015). This is based on an analysis that the ejection of 0.1 $M_\odot$ of Fe leads in a CCSN remnant to [Fe/H]≈-2.7 (Ryan et al. 1996). If only 10% or 1% of supernova ejecta contribute to the formation of the next stars, one expects, therefore, [Fe/H] values as small as -4 or -5. More extended recent chemical evolution studies take this into account in a more general approach (see e.g. Kobayashi et al. 2020; van de Voort et al. 2020, 2022). Based on Ryan et al. (1996) a starting hypothesis could be that stars with metallicities below -2.5 might be interpreted as the result from the contribution of only a single nucleosynthesis event (although this will be questioned later on). Do therefore low-metallicity stars display the results of individual, but different, astrophysical events?
One of the major questions about r-process contributions to solar abundances is whether they are universal and stem from a unique astrophysical site. Early signs from low-metallicity stars seemed to show such a unique

r-process pattern, therefore pointing to a universal site (Burris et al. 2000). This interpretation started to become questionable when actinide-boost stars were observed (Cayrel et al. 2001) and the first limited-r stars were discovered (Honda et al. 2006). This could be explained by just seeing abundance patterns of the events discussed in the previous section. Fig. 7 shows that observations of low metallicity stars indicate the existence of a weak or limited r-process (dependent on the [Eu/Fe]-ratio), categorized into limited-r (with [Eu/Fe]<0 to 0.3), and r-enriched (r-I with [Eu/Fe]<1 and r-II with [Eu/Fe]>1) stars. Most r-process enhanced stars, however, show a close to solar r-process pattern. This goes together with a variation of e.g., the Sr/Eu ratio, ranging from about 1120 down to 0.5 (Hansen et al. 2018), and indicating the different decline of the abundance curve as a function of A. Some of the r-process enriched stars show an "actinide boost", i.e. their Th or U to Eu ratio is supersolar (see e.g., Roederer et al. 2010; Holmbeck et al. 2018, 2019b,a).

The impact of essentially three types of predicted patterns, a weak or limited r-process, a strong solar-type r-process, and an actinide-boosted r-process has been treated in galactic chemical evolution models (see e.g., Matteucci et al. 2014; Wehmeyer et al. 2015; Cescutti et al. 2015; van de Voort et al. 2020; Perego et al. 2021; Cowan et al. 2021; Thielemann et al. 2022; van de Voort et al. 2022; Farouqi et al. 2022), which can also treat the impact of rare events (see Fig. 7). Whether the latter two types are produced in different sites or result from variations within the same site (e.g., neutron star mergers with different properties) is still debated. A promising approach is to look for correlations among different elements.

3.1. Statistical abundance analysis

If abundance patterns of low-metallicity stars result from the pollution by only a single type of event, this would cause correlations between those elements resulting from the originating event (for a recent example see Yong et al. 2021). Such correlations (i.e. linear relations, respective constant ratios, between their abundances) underline the co-production of these elements. If (at low metallicities) elemental abundances are interpreted as imprints of individual explosions, a large scatter as a function of [Fe/H] points to either rare events with different amounts of admixtures and/or to different types of events with strong variations in their ejected composition. The variation in [Eu/Fe] vs. [Fe/H] could be interpreted by such explanations, the large Sr/Eu in limited-r stars vs. the low values in r-enriched stars hints at different types of events (see Fig.7).

In late phases of galactic evolution a large number of different events have taken place,

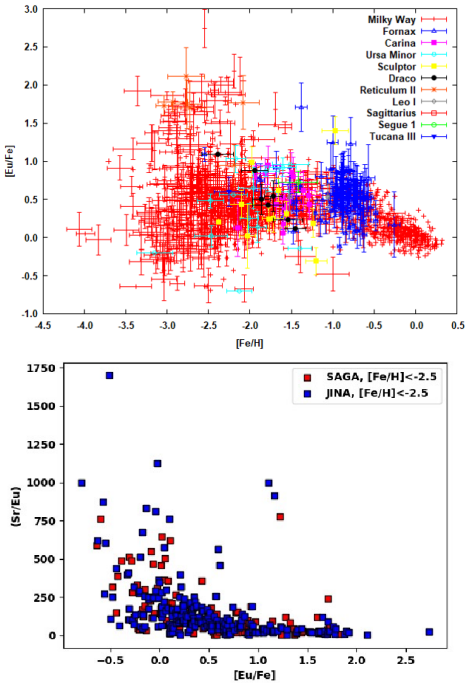

Fig. 7. Top: [Eu/Fe] ratios of 1572 stars with Eu detections from the SAGA database (Suda et al. 2008). A huge scatter can be observed before at about [Fe/H]= −2 an averaging (smaller spread) sets in, which continues with a different gradient when SNe Ia start to contribute at −1. Bottom: Sr/Eu ratios for all stars with [Fe/H]< −2.5 show a drastic change at about [Eu/Fe]= 0 − 0.3, i.e. the division between limited-r stars and r-enriched stars. Image reproduced with permission from Farouqi et al. (2022), copyright by authors.

leading via superpositions and admixtures of the ejecta to a strongly decreased scatter in abundance ratios. The analysis of the observed abundance patterns in low-metallicity stars can be aided by three methods in order to gain insight into the possibly different origins of the r-process: cluster analysis, rank tests, and correlations.

3.2. Clustering

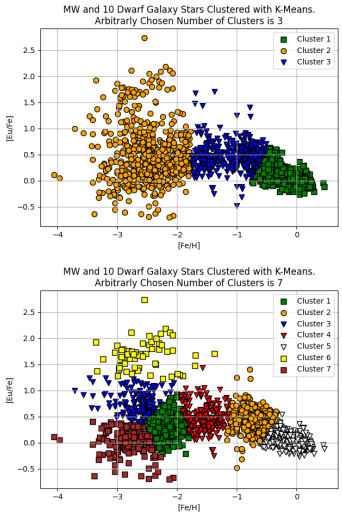

Fig. 8. 3-cluster and 7-cluster analysis of [Eu/Fe] ratios as a function of [Fe/H], see text. Image reproduced with permission from Farouqi et al. (2022), copyright by authors.

Cluster analysis is a statistical technique to identify how data can be grouped because of characteristics they have in common (Everitt et al. 2011). One method is the K-means Clustering: it distributes data into K mutually exclusive clusters so that with a given measure data points are as close to each other as possible within each cluster, while at the same time they are as far from other clusters as possible. In the 3-cluster analysis of the Eu vs. Fe abundances of Fig.8 one can recognize in cluster 1 the low-metallicity stars where the large scatter indicates contributions from individual rare and/or different events, in cluster 2 for [Fe/H]>-2 that already an averaging/mixing of event products sets in and the scatter becomes small, and in cluster 3 that Fe is contributed also from SNe Ia and changes the general Eu/Fe trend. In the 7-cluster analysis one recognizes different stages of the approach to averaging/mixing (clusters 1, 2, 4), and for low-metallicity stars with [Fe/H]<-2.5 three clusters (3, 6, 7) with properties close to the observational limited-r, r-I, and r-II classes of [Eu/Fe]<0-0.3, < 1, and >1.

3.3. Rank Test

Fig.9 shows examples for utilizing a single random number generator X and ordering the values according to their size, giving them integer entries (ranks). This leads to a linear relation between the random numbers and their ranks (see the orange line in top panel). The blue line results when utilizing two random number generators, adding their values $Y = X_1 + X_2$, and plotting Y as a function of its ranks. It deviates from a linear relation between Y and its ranks, at low ranks depending on the fact whether the second contribution includes many low-value entries, at high ranks depending on the number of high-value entries. If one applies this method to abundance observations of individual elements as a function of rank, it can indicate whether only one type of nucleosynthesis source or two or several contributed.

Eu abundances versus their corresponding ranks are displayed in Fig.9 (middle). The fit deviates strongly from a linear behavior at high Eu ranks. This argues for a superposition with an additional Eu source, especially responsible for the high Eu abundances. A different behavior can be noticed for Fe abundances versus their corresponding ranks. Fig.9 (bottom) shows a close to linear relation. This would argue for a single or dominating production site (explosive Si-burning in CCSNe?).

If one performs a similar rank test for Th in r-enriched stars (r-I and r-II), it can be noticed that a superposition of two types of events is required. But one finds a linear rank relation when plotting Th abundances as a function of their ranks separately for r-I and r-II stars (with a slight scatter). Thus, r-I and r-II

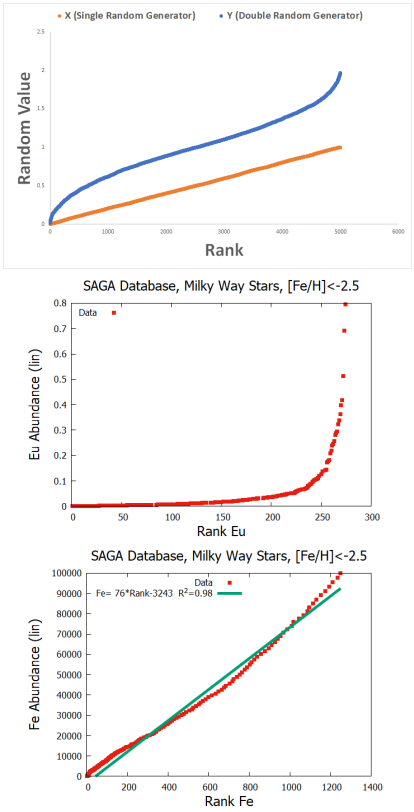

Fig. 9. Top: data ordered along their ranks from a single number generator X, showing (a) a linear relation between X-values and their rank, and (b) the sum $X_1 + X_2$ of two single number generators vs. its rank, deviating from a linear relationship. Middle: Eu abundances vs. their rank for low-metallicity stars with [Fe/H]<-2.5, at high ranks (i.e. high Eu abundances) one recognizes an additional/different strong contribution. Bottom: The same for Fe abundances, displaying almost a linear relationship, pointing to one identical source, but at low as well as high Fe abundances slight deviations are seen. Image reproduced with permission from Farouqi et al. (2022), copyright by authors.

stars seem each to be dominated by contributions from one specific type of event, each of them being responsible for their Th production independently. This is not the case when performing a rank tests for Eu in r-I and r-I stars. Opposite to Th, Eu does not show a linear rank relation, when considering r-I and r-II stars separately. This suggests that also among r-enriched (strong r-process r-I and r-II) stars weak r-process events "spill in" an additional Eu contribution (for details see Farouqi et al. 2022).

3.4. Correlations

When analyzing data sets of (x,y) points, the Pearson correlation coefficient measures a possible linear relationship (constant ratio) between their values. In such a case the value of the correlation is either +1 or -1, depending on whether a linear fit to this relation has a positive or negative slope. The correlation measures also a possible noisiness, the extreme case of a linear fit with a huge χ^2, i.e. which does not fit the data at all, stands for a correlation value of 0. The Spearman correlation coefficient measures correlations in a slightly "milder" way, based on ranks rather than a linear relation. A deviation of both methods indicates the start of a different correlation pattern (Tamhane & Dunlop 2000; Spiegelhalter 2019).
When applying this method to correlations between Eu and Fe the results are shown for the Pearson and Spearman correlation coefficients in Fig.10. Among the limited-r stars two types of contributions seem to dominate, seen in regimes 1 and 2 with a high correlation between Fe and Eu, indicating the co-production of both elements in the responsible events. In regime 3 (r-enriched stars) a vanishing correlation is strongly supporting sites which produce heavy r-process elements uncorrelated (i.e. not co-produced) with Fe, i.e. strong r-process events (without - or possibly with - an actinide boost, see Fig.4).

4. Quantitative imprints of r-process sites in low-metallicity stars

In section 2 the production of trans-Fe elements were presented for regular CCSNe, QD supernovae, MR SNe, collapsars/hypernovae and compact binary mergers. Regular CCSNe with a νp- and possibly a very weak r-process produce elements like Sr, Y, Zr at lowest metallicities (an explanation for the LEPP process?, Travaglio et al. 2004) but no Eu. [For an ad-

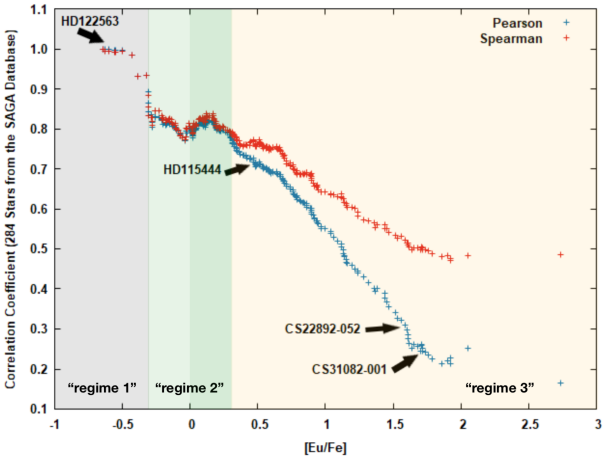

Fig. 10. Shown are the Pearson and Spearman correlation coefficients for low-metallicity stars ([Fe/H <-2.5) from the JINAbase database (Abohalima & Frebel 2018), considering stars in an [Eu/Fe] interval with its upper limit displayed on the x-axis. We see for limited-r stars of regime 1 and 2 a high correlation, indicating Fe and Eu co-production, while for r-enriched stars of regime 3 the correlations vanish, arguing for separate nucleosynthesis sources for the Fe and Eu found in these stars. Four typical stars (HD122563, limited-r), HD115444 (r-enriched, r-I), CS22892-052 (r-enriched, r-II), and CS31082-001 (r-enriched, r-II with actinide boost) are displayed as well. Image reproduced with permission from Farouqi et al. (2022), copyright by authors.

ditional contribution from the weak s-process in rotating massive stars see e.g. Frischknecht et al. (2016) and Cescutti et al. (2021)] . Farouqi et al. (2022) find a strong correlation of these elements with Fe (dominated in low metallicity stars by CCSNe). Quark deconfinement supernovae and magneto-rotational supernovae are mainly responsible for a weak r-process (with the - although small - production of Eu), which would lead to a strong correlation of Eu and Fe, as found in limited-r stars of regime 1 and 2 of Fig.10. Farouqi et al. (2022) find, by utilizing the predictions for QD SNe (Fischer et al. 2020) as well as for two sets of magneto-rotational MR SNe 1 and 2 (Nishimura et al. 2017; Reichert et al. 2021), that QD and MR SNe can reproduce the regime 1 and 2 Sr/Eu observations well, but in order to reproduce also the observed Sr/Fe and Eu/Fe values, an additional contribution of 0.1 $M_\odot$ of Fe is required by 200-300 regular CCSNe per QD SN, while 10 regular CCSNe per MR SN are needed. The latter is comparable with the magnetar fraction of neutron stars and clearly points to MR SNe as well.

The rank tests for Th, discussed in 3.3, have shown that the strong r-process events fall into two subcategories without and with an actinide boost. The question which physical conditions lead to such an actinide boost has been raised in section 2.3. Actinide-boost stars with Th/Eu supersolar (>0.42, (Lodders 2021)) exist mostly among r-II stars. This answers the question how we can relate the observed behavior to strong r-process events of regime 3 by identifying them with NS-mergers and BH accretion tori outflows, e.g. collapsars or compact binary mergers with fast black hole formation. This is consistent with the separate rank tests for Th in r-I and r-II stars. Independent of the actinide boost question, the predicted Eu production for these events (about $10^{-6}M_\odot$ vs. $10^{-4}M_\odot$, when utilizing the results from (Côté et al. 2017; Siegel et al. 2019)), can be tested in combination with negligible Fe production for NS mergers or about $0.5M_\odot$ of Fe for the latter collapsar case. In order to reproduce the observed Eu/Fe values in r-I stars (by NS mergers) and r-II stars (by collapsars) requires in both cases the addition of about ≈120 x $0.1M_\odot$

of Fe from CCSNe, i.e. they need to occur with a frequency of a few permille of CCSNe (consistent with Rosswog et al. 2017).

This analysis answers the question whether the large scatter in r-process abundances with respect to those of other elements (e.g. Eu vs. Fe) at low metallicities is only the result of inhomogeneous admixture from one type of rare events (i.e. compact binary mergers, Holmbeck et al. 2021)), or does it point to different origins? Such questions have been addressed in many galactic chemical evolution studies (e.g. Wehmeyer et al. 2015; Cescutti et al. 2015; Kobayashi et al. 2020; van de Voort et al. 2020; Cescutti et al. 2021; van de Voort et al. 2022; Van der Swaelmen et al. 2022). We hope that with the analysis presented in this review we showed with the cluster, rank, and correlation / no correlation tests that different sources resulting either in a weak r-process with Fe co-production or a strong r-process with no or negligible Fe co-production are responsible. The effect that the r-process (or Eu) production in these events (QD and MR SNe, NS mergers, collapsars/black hole accretion tori) increases among these categories by about a factor of 10 for each, permits an explanation of the limited-r, r-I, and r-II patterns, combined with the inhomogeneous evolution in the early Galaxy. The onset of observations available for these subcategories at different metallicities from [Fe/H] <-4 to -3 hints also at the different occurrence frequency of these events (see Fig.26 in Farouqi et al. (2022), underlining that more frequent r-process contributions occurred before neutron star mergers).

Acknowledgements. We thank the authors of the publicly available observational SAGA and JINA data bases (Suda et al. 2008; Abohalima & Frebel 2018). Furthermore, the COST actions ChETEC (Chemical Elements as Tracers of the Evolution of the Cosmos, CA16117), GWverse (Gravitational waves, black holes and fundamental physics, CA16104), and Pharos (The multi-messenger physics and astrophysics of neutron stars, CA16214) as well as the International Research Network for Nuclear Astrophysics (IReNA) provided an inspiring atmosphere for thoughts along the lines discussed here.

References

Abbott, B. P. et al. 2017, Phys. Rev. Lett., 119, 161101
Abohalima, A. & Frebel, A. 2018, ApJS, 238, 36
Arcones, A. & Thielemann, F.-K. 2022, Astron. Astrophys. Rev., 30, xxx
Barnes, J., Zhu, Y. L., Lund, K. A., et al. 2021, ApJ, 918, 44
Bauswein, A., Just, O., Janka, H.-T., & Stergioulas, N. 2017, ApJ, 850, L34
Beloborodov, A. M. 2003, ApJ, 588, 931
Burris, D. L., Pilachowski, C. A., Armandroff, T. E., et al. 2000, ApJ, 544, 302
Burrows, A. 2013, Rev. Mod. Phys. , 85, 245
Burrows, A., Dessart, L., Livne, E., Ott, C. D., & Murphy, J. 2007, Astrophys. J., 664, 416
Burrows, A. & Vartanyan, D. 2021, Nature, 589, 29
Cayrel, R., Hill, V., Beers, T. C., et al. 2001, Nature, 409, 691
Cescutti, G., Morossi, C., Franchini, M., et al. 2021, A&A, 654, A164
Cescutti, G., Romano, D., Matteucci, F., Chiappini, C., & Hirschi, R. 2015, A&A, 577, A139
Chen, W. & Beloborodov, A. M. 2007, ApJ, 657, 383
Côté, B., Belczynski, K., Fryer, C. L., et al. 2017, 836, 230
Cowan, J. J., Sneden, C., Lawler, J. E., et al. 2021, Rev. Mod. Phys. , 93, 015002
Curtis, S., Ebinger, K., Fröhlich, C., et al. 2019, ApJ, 870, 2
Curtis, S., Mösta, P., Wu, Z., et al. 2022, MNRASarXiv:2112.00772
Duflo, J. & Zuker, A. P. Phys. Rev. C 1995, 52, R23
Ebinger, K., Curtis, S., Ghosh, S., et al. 2020, ApJ, 888, 91
Eichler, D., Livio, M., Piran, T., & Schramm, D. N. 1989, Nature, 340, 126
Eichler, M., Sayar, W., Arcones, A., & Rauscher, T. 2019, ApJ, 879, 47
Evans, P. A. et al. 2017, Science, 358, 1565
Everitt, B. S., Landau, S., Leese, M., & Stahl, D. 2011, Cluster Analysis, 5th Edition, Wiley Series in Probability and Statistics (New York: Wiley)

Farouqi, K., Thielemann, F.-K., Rosswog, S., & Kratz, K.-L. 2022, A&A, 663, A70
Fernández, R., Tchekhovskoy, A., Quataert, E., Foucart, F., & Kasen, D. 2019, MNRAS, 482, 3373
Fischer, T., Sagert, I., Pagliara, G., et al. 2011, ApJS, 194, 39
Fischer, T., Wu, M.-R., Wehmeyer, B., et al. 2020, ApJ, 894, 9
Frischknecht, U., Hirschi, R., Pignatari, M., et al. 2016, MNRAS, 456, 1803
Fröhlich, C., Martínez-Pinedo, G., Liebendörfer, M., et al. 2006, Phys. Rev. Lett., 96, 142502
Fujibayashi, S., Kiuchi, K., Wanajo, S., et al. 2022, arXiv e-prints arXiv:2205.05557
Ghosh, S., Wolfe, N., & Fröhlich, C. 2022, ApJ, 929, 43
Greiner, J. et al. 2015, Nature, 523, 189
Hansen, T. T., Holmbeck, E. M., Beers, T. C., et al. 2018, ApJ, 858, 92
Holmbeck, E. M., Beers, T. C., Roederer, I. U., et al. 2018, ApJ, 859, L24
Holmbeck, E. M., Frebel, A., McLaughlin, G. C., et al. 2019a, ApJ, 881, 5
Holmbeck, E. M., Frebel, A., McLaughlin, G. C., et al. 2021, ApJ, 909, 21
Holmbeck, E. M., Sprouse, T. M., Mumpower, M. R., et al. 2019b, ApJ, 870, 23
Honda, S., Aoki, W., Ishimaru, Y., Wanajo, S., & Ryan, S. G. 2006, ApJ, 643, 1180
Horowitz, C. J. et al. 2019, J. Phys. G , 46, 083001
Janka, H.-T., Melson, T., & Summa, A. 2016, Annu. Rev. Nucl. Part. Sci. , 66, 341
Ji, A. P., Drout, M. R., & Hansen, T. T. 2019, ApJ, 882, 40
Just, O., Bauswein, A., Pulpillo, R. A., Goriely, S., & Janka, H.-T. 2015, MNRAS, 448, 541
Kasen, D., Metzger, B., Barnes, J., Quataert, E., & Ramirez-Ruiz, E. 2017, Nature, 551, 80
Kasliwal, M. M., Kasen, D., Lau, R. M., et al. 2022, MNRAS Lett., 510, L7
Kobayashi, C., Karakas, A. I., & Lugaro, M. 2020, ApJ, 900, 179
Korobkin, O., Rosswog, S., Arcones, A., & Winteler, C. 2012, MNRAS, 426, 1940
Kotake, K., Takiwaki, T., Suwa, Y., et al. 2012, Advances in Astronomy, 2012, 428757
Kramer, M. 2009, in IAU Symposium, Vol. 259, Cosmic Magnetic Fields: From Planets, to Stars and Galaxies, ed. K. G. Strassmeier, A. G. Kosovichev, & J. E. Beckman, 485–492
Kuroda, T., Arcones, A., Takiwaki, T., & Kotake, K. 2020, ApJ, 896, 102
Lattimer, J. M. & Schramm, D. N. 1974, ApJ, 192, L145
Lattimer, J. M. & Schramm, D. N. 1976, ApJ, 210, 549
Lee, W. H. & Ramirez-Ruiz, E. 2007, New J. Phys., 9, 17
Lodders, K. 2021, Space Sci. Rev., 217, 44
Lund, K. A., Engel, J., McLaughlin, G. C., et al. 2022, arXiv e-prints, arXiv:2208.06373
Martin, D., Perego, A., Arcones, A., et al. 2015, ApJ, 813, 2
Matteucci, F., Romano, D., Arcones, A., Korobkin, O., & Rosswog, S. 2014, MNRAS, 438, 2177
McLaughlin, G. C. & Surman, R. 2005, Nucl. Phys. A, 758, 189
Metzger, B. D. 2019, Living Rev. Relativ., 23, 1
Metzger, B. D., Martínez-Pinedo, G., Darbha, S., et al. 2010, MNRAS, 406, 2650
Miller, J. M., Ryan, B. R., Dolence, J. C., et al. 2019, Phys. Rev. D, 100, 023008
Miller, J. M., Sprouse, T. M., Fryer, C. L., et al. 2020, ApJ, 902, 66
Mösta, P., Richers, S., Ott, C. D., et al. 2014, ApJ, 785, L29
Mösta, P., Roberts, L. F., Halevi, G., et al. 2018, ApJ, 864, 171
Müller, B. 2016, Publ. Astron. Soc. Aust. , 33, e048
Müller, B. 2020, Living Rev. Comput. Astrophys., 6, 3
Nishimura, N., Sawai, H., Takiwaki, T., Yamada, S., & Thielemann, F.-K. 2017, ApJ, 836, L21
Nishimura, N., Takiwaki, T., & Thielemann, F.-K. 2015, ApJ, 810, 109
Nomoto, K., Tanaka, M., Tominaga, N., & Maeda, K. 2010, New Astron. Rev. , 54, 191
Obergaulinger, M., Cerdá-Durán, P., Müller, E., & Aloy, M. A. 2009, A&A, 498, 241

Obergaulinger, M., Janka, H.-T., & Aloy, M. A. 2014, MNRAS, 445, 3169
Perego, A., Hempel, M., Fröhlich, C., et al. 2015, ApJ, 806, 275
Perego, A., Thielemann, F.-K., & Cescutti, G. 2021, in Handbook of Gravitational Wave Astronomy, ed. C. Bambi, S. Katsanevas, & K. D. Kokkotas (Singapore: Springer), 1
Perego, A., Vescovi, D., Fiore, A., et al. 2022, ApJ, 925, 22
Radice, D., Abdikamalov, E., Ott, C. D., et al. 2018, J. Phys. G , 45, 053003
Reichert, M., Obergaulinger, M., Aloy, M. Á., et al. 2022, MNRASarXiv:2206.11914
Reichert, M., Obergaulinger, M., Eichler, M., Aloy, M. Á., & Arcones, A. 2021, MNRAS, 501, 5733
Roederer, I. U., Sneden, C., Lawler, J. E., & Cowan, J. J. 2010, ApJ, 714, L123
Rosswog, S., Feindt, U., Korobkin, O., et al. 2017, Class. Quantum Gravity, 34, 104001
Rosswog, S. & Korobkin, O. 2022, Annalen der Physik, arXiv:2208.14026
Rosswog, S., Sollerman, J., Feindt, U., et al. 2018, A&A, 615, A132
Ryan, S. G., Norris, J. E., & Beers, T. C. 1996, ApJ, 471, 254
Shibata, M., Fujibayashi, S., & Sekiguchi, Y. 2021, Phys. Rev. D, 104, 063026
Shibata, M. & Hotokezaka, K. 2019, Annu. Rev. Nucl. Part. Sci. , 69, 41
Siegel, D. M., Barnes, J., & Metzger, B. D. 2019, Nature, 569, 241
Siegel, D. M. & Metzger, B. D. 2017, Phys. Rev. Lett., 119, 231102
Siegel, D. M. & Metzger, B. D. 2018, ApJ, 858, 52
Spiegelhalter, D. 2019, The art of statistics (Milton Keynes: Penguin Random House)
Suda, T., Katsuta, Y., Yamada, S., et al. 2008, PASJ, 60, 1159
Surman, R. & McLaughlin, G. C. 2004, ApJ, 603, 611
Surman, R., McLaughlin, G. C., & Hix, W. R. 2006, ApJ, 643, 1057
Takiwaki, T., Kotake, K., & Sato, K. 2009, ApJ, 691, 1360
Tamhane, A. & Dunlop, D. 2000, Statistics and Data Analysis (Upper Saddle River: Prentice-Hall)
Thielemann, F.-K., Eichler, M., Panov, I. V., & Wehmeyer, B. 2017, Annu. Rev. Nucl. Part. Sci. , 67, 253
Thielemann, F.-K., Farouqi, K., Rosswog, S., & Kratz, K.-L. 2022, Eur. Phys. J. Web Conf., 260, 09002
Thielemann, F.-K., Wehmeyer, B., & Wu, M.-R. 2020, J. Phys. Conf. Ser., 1668, 012044
Travaglio, C., Gallino, R., Arnone, E., et al. 2004, ApJ, 601, 864
van de Voort, F., Pakmor, R., Bieri, R., & Grand, R. J. J. 2022, MNRAS, 512, 5258
van de Voort, F., Pakmor, R., Grand, R. J. J., et al. 2020, MNRAS, 494, 4867
Van der Swaelmen, M., Viscasillas Vázquez, C., Cescutti, G., et al. 2022, arXiv e-prints, arXiv:2207.14747
Varma, V., Mueller, B., & Schneider, F. R. N. 2022, arXiv e-prints, arXiv:2204.11009
Vartanyan, D., Coleman, M. S. B., & Burrows, A. 2022, MNRAS, 510, 4689
Wanajo, S., Sekiguchi, Y., Nishimura, N., et al. 2014, ApJ, 789, L39
Watson, D., Hansen, C. J., Selsing, J., et al. 2019, Nature, 574, 497
Wehmeyer, B., Pignatari, M., & Thielemann, F.-K. 2015, MNRAS, 452, 1970
Winteler, C., Käppeli, R., Perego, A., et al. 2012, ApJ, 750, L22
Woosley, S. E. & Bloom, J. S. 2006, ARA&A, 44, 507
Wu, M.-R., Barnes, J., Martínez-Pinedo, G., & Metzger, B. D. 2019, Phys. Rev. Lett., 122, 062701
Wu, M.-R., Fernández, R., Martínez-Pinedo, G., & Metzger, B. D. 2016, MNRAS, 463, 2323
Wu, M.-R. et al. 2017, unpublished
Yong, D., Kobayashi, C., Da Costa, G. S., et al. 2021, Nature, 595, 223
Zhu, Y. et al. 2018, ApJ, 863, L23